

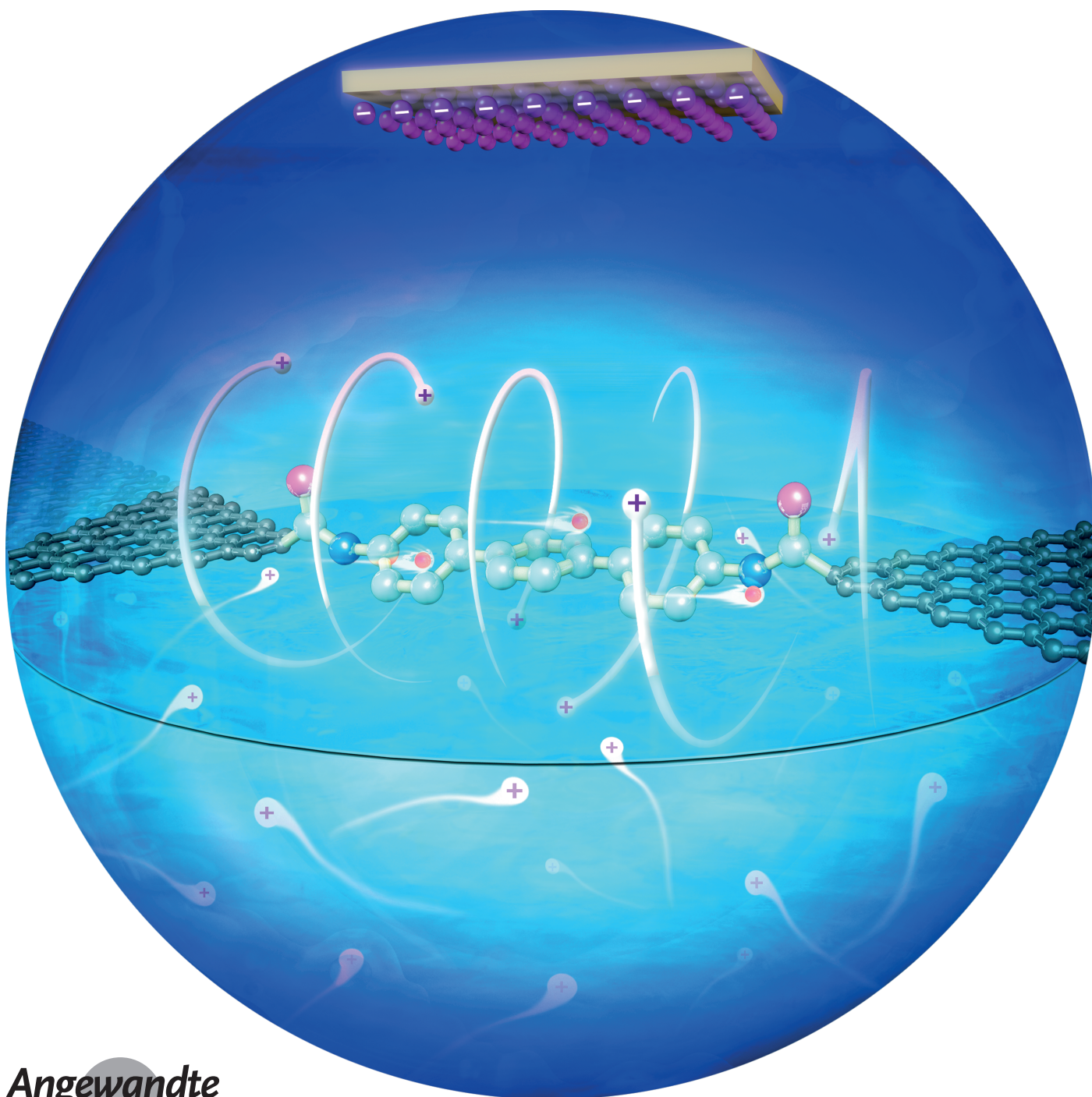
Single-Molecule Junctions

International Edition: DOI: 10.1002/anie.201807465

German Edition: DOI: 10.1002/ange.201807465

# Tuning Charge Transport in Aromatic-Ring Single-Molecule Junctions via Ionic-Liquid Gating

Na Xin<sup>+</sup>, Xingxing Li<sup>+</sup>, Chuancheng Jia<sup>+</sup>, Yao Gong, Mingliang Li, Shuopei Wang, Guangyu Zhang, Jinlong Yang,<sup>\*</sup> and Xuefeng Guo<sup>\*</sup>



**Abstract:** Achieving gate control with atomic precision, which is crucial to the transistor performance on the smallest scale, remains a challenge. Herein we report a new class of aromatic-molecular nanotransistors based on graphene–molecule–graphene single-molecule junctions by using an ionic-liquid gate. Experimental phenomena and theoretical calculations confirm that this ionic-liquid gate can effectively modulate the alignment between molecular frontier orbitals and the Fermi energy level of graphene electrodes, thus tuning the charge-transport properties of the junctions. In addition, with a small gate voltage ( $|V_G| \leq 1.5$  V) ambipolar charge transport in electrochemically inactive molecular systems ( $E_G > 3.5$  eV) is realized. These results offer a useful way to build high-performance single-molecule transistors, thus promoting the prospects for molecularly engineered electronic devices.

Stimulated by the initial proposal that a single molecule could be used as the functional unit in the circuit of electronic devices,<sup>[1]</sup> researchers have been making great efforts to realize various functionalities at the single-molecule level,<sup>[2]</sup> as well as to probe and understand the intrinsic properties of materials at the atomic/molecular scale.<sup>[3]</sup> The development of single-molecule transistors, in which a single molecule is sandwiched between two nanogapped electrodes while the energy levels of the resulting molecular bridge are controlled by a third proximal electrode,<sup>[4]</sup> is particularly attractive because they form a basic element in molecular nanocircuits for future practical applications.<sup>[5]</sup> Because the inherent characteristics of molecular orbital energy levels is one of the most critical factors influencing charge transport in molecular junctions, this three-terminal device architecture also provides a universal strategy to explore quantum transport and novel physical phenomena of single molecules.<sup>[5,6]</sup> In addition to Coulomb blockade<sup>[7]</sup> and Kondo resonance,<sup>[3f]</sup> three-terminal devices have been employed to probe vibron-assisted charge transport in single-molecule junctions such as Frank–Condon blockade,<sup>[8]</sup> and to reveal the fine structure of individual single-molecule magnets and the presence of magnetic anisotropy.<sup>[2d,7,9]</sup> As gate electrode allows the electrons to repel and attract from the molecules, it can be utilized to oxidize and reduce molecules, thus

enabling the investigation of the transport properties of molecules at different charge states.<sup>[10]</sup>

Several approaches have been developed to fabricate molecular junctions with a gate electrode in a transistor configuration. In general, there are two main kinds:<sup>[4,11]</sup> one is back gate, which is well used for electromigrated molecular junctions and mechanically controllable break junctions (MCBJ);<sup>[12]</sup> the other is electrochemical gate, most widely used in scanning tunneling microscope (STM) break junctions.<sup>[13]</sup> Though significant observations were achieved, we cannot ignore the limits. For back gate, the molecule-gate coupling is generally weak, thus a high gate voltage is needed to apply an efficient electric field to the molecular junction, which is energy-consuming. Owing to some thermally-induced effects, most transistor behaviors were only observed in vacuum at low temperatures. In addition, at present because of the technique limits, it is difficult to precisely control the molecule-gate coupling, resulting in poor reproducibility. It seems that electrochemical gate is able to compensate the deficiency of back gate.<sup>[13]</sup> Though electrochemical gate can result in a strong and reproducible gate field to modulate charge transport across single molecules; its liquid state and complex configuration prevent it from fundamental research at low temperatures (owing to the coagulation of the aqueous electrolyte solution) and further step toward real applications.

To overcome the above-discussed problems, we introduced an ionic liquid as a gate dielectric to construct single-molecule transistors (Figures 1 a,b), by using graphene–molecule–graphene single-molecule junctions (GMG-SMJs) previously developed in our group.<sup>[14]</sup> As a result of the good stability of the graphene electrode materials and the covalent amide linkages, the contacts of the junctions are robust, thus ensuring the exploration of the device function from the intrinsic properties of the connected molecule. In addition, the two-dimensional nature of graphene results in weaker screening of a gate electric field in comparison with three-dimensional metal electrodes. We chose an ionic liquid as the dielectric layer because it is an established and effective strategy to modulate charge transport in semiconductor devices.<sup>[15]</sup> First of all, the applied gate voltage drops across a geometrical electrical double layer (EDL) of about 7.5 Å thickness with a large capacitance (Figure 1 b), which is determined by the size of cation and anion of used ionic liquid, thus leading to a strong electric field to single-molecule junctions. Different from the aqueous electrolyte solution, ionic liquid has a large liquid temperature range (melting point is ca. 180 K),<sup>[16]</sup> and can keep its EDL unchanged even when it freezes. In single-molecule transistors, the gate responses depend on several key factors including the strength of molecule–electrode interface coupling, the gate coupling coefficient, and the dominant molecular orbital property. Previous reports observed that molecules that conduct through the lowest unoccupied molecular orbital (LUMO, n-type) show an increase in conductance with positive gate potentials and a decrease in conductance with negative gate potentials, while molecules that conduct through the highest occupied molecular orbital (HOMO, p-type) show the opposite trend.<sup>[17]</sup> In the study of molecular

[\*] Dr. N. Xin,<sup>[†]</sup> Dr. C. Jia,<sup>[†]</sup> Y. Gong, Dr. M. Li, Prof. Dr. X. Guo  
Beijing National Laboratory for Molecular Sciences, State Key  
Laboratory for Structural Chemistry of Unstable and Stable Species  
College of Chemistry and Molecular Engineering, Peking University  
Beijing 100871 (P. R. China)

E-mail: guoxf@pku.edu.cn

Dr. X. Li,<sup>[†]</sup> Prof. Dr. J. Yang

Hefei National Laboratory for Physical Sciences at Microscale  
University of Science and Technology of China  
Hefei, Anhui 230026 (P. R. China)

E-mail: jlyang@ustc.edu.cn

S. Wang, Prof. G. Zhang

Institute of Physics, Chinese Academy of Science  
Beijing 100190 (P. R. China)

[†] These authors contributed equally to this work.

Supporting information and the ORCID identification number(s) for the author(s) of this article can be found under:  
<https://doi.org/10.1002/anie.201807465>.

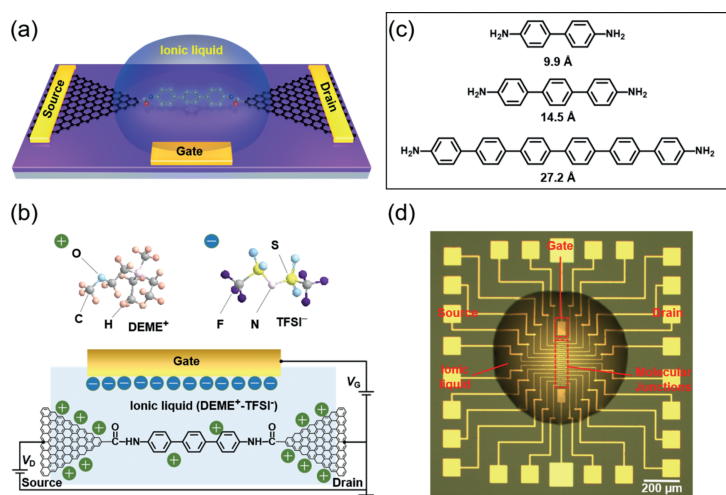


**Figure 1.** Graphene–molecule–graphene single-molecule junctions with ionic-liquid gate dielectric. a), b) Schematic illustration for the setup of single-molecule transistors and molecular structures for  $\text{DEME}^+$  cation and  $\text{TFSI}^-$  anion, which have similar sizes, approximately 7.5 Å. c) Molecular structures of biphenyl, triphenyl, and hexaphenyl molecules with amine ends as the anchoring group. d) Optical image of an array of GMG-SMJs with common gate electrodes at the middle top and middle bottom, covered with a small droplet of ionic liquid.

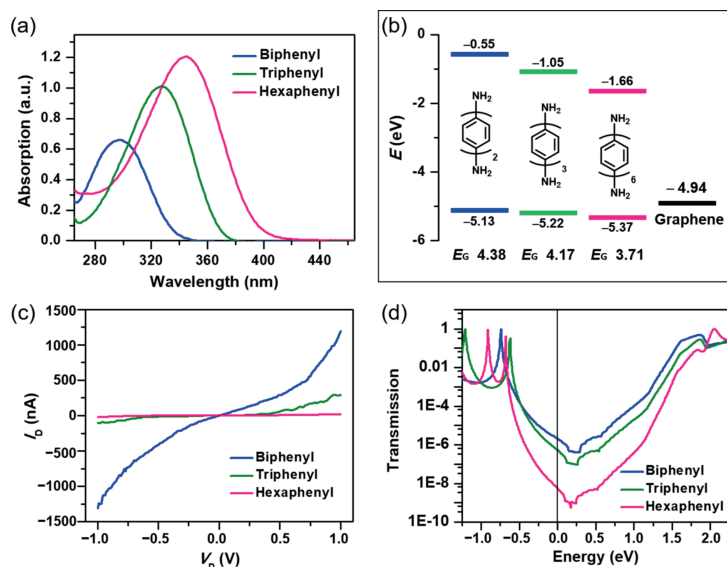
junctions with small HOMO–LUMO energy gaps, such as substituted perylenetetracarboxylic diimide molecular junction with an energy gap of around 1.72 eV, switching between electron- and hole-dominated charge transports as a function of gate voltage can be observed, which demonstrated a single-molecule ambipolar field-effect transistor.<sup>[18]</sup> In addition, for electrochemically active pyrrolo-tetrathiafulvalene or porphyrin molecular junctions, the ambipolar conductance phenomenon was also observed when the gate voltage swept through two redox transitions.<sup>[10b,d]</sup> Herein, we demonstrate tunable charge transport in GMG-SMJs with an ionic liquid gate, which affords the ambipolar conductance behavior in the electrochemically inactive molecular systems with a large HOMO–LUMO energy gap (Figure 1c), owing to the adjustment of aligning the dominant conducting molecular orbitals (HOMO or LUMO) and the Fermi energy level of graphene electrodes.

Figure 1d shows the optical photograph of an array of single-molecule transistors. By using nano-gapped graphene point contacts formed through a dash-line lithographic method described in detail elsewhere,<sup>[19]</sup> individual molecules were covalently linked to graphene electrodes with amide bonds to form single-molecule junctions (details of device fabrication are described in the Supporting Information). At last, a small droplet of ionic liquid covering the array of graphene-based molecular junctions and the gate. To produce the symmetric EDLs when the opposite gate voltages are applied, we chosen the ionic liquid consisting of positive and negative ions with the

similar size, N,N-diethyl-N-(2-methoxyethyl)-N-methylammonium bis(trifluoromethylsulfonyl)imide (DEME-TFSI), as shown in Figure 1b.

To investigate the efficiency of ionic liquid gating, we designed three electrochemically inactive phenyl-based molecular structures with different molecular lengths (Figure 1c) to build single-molecule transistors. The biphenyl and triphenyl molecular materials were purchased from Alfa and TCI (without further purification), respectively. The hexaphenyl molecular material was synthesized by following the procedure detailed in the Supporting Information. These three molecules differ in the number of phenyl rings and thus the molecular length. Because the EDL thickness is comparable to the molecular scale, the molecular length is expected to play a significant role in realizing effective gate control. Previous studies proved that in fully conjugated molecular systems, the HOMO–LUMO gap decreases as the conjugated length increases.<sup>[20]</sup> The absorption spectra in Figure 2a show a clear decrease of the optical energy gap as the aromatic chain becomes longer, which is consistent with the calculated energy diagram in Figure 2b. Correspondingly, the conductance of the single-molecule junctions decreases with the molecular length increases (Figure 2c and Supporting Information,

Figure S2): The conductance value at 1 V follows the exponential formula  $G \propto \exp(-\beta L)$ , with  $\beta = 0.23 \text{ \AA}^{-1}$  or 0.99/phenyl, which demonstrates the tunneling transport behaviors with molecular length dependence<sup>[21]</sup> (Supporting Information, Figure S3). Such conductance differences can



**Figure 2.** Charge-transport properties and energy levels of biphenyl, triphenyl, and hexaphenyl single-molecule junctions. a) Normalized UV/Vis absorption spectra for all three molecules measured in dimethyl formamide. b) Calculated molecular orbital energy levels of isolated molecules, and the graphene Fermi level deduced from experimental results. c)  $I$ – $V$  characteristics of biphenyl/triphenyl/hexaphenyl-reconnected molecular junctions measured at room temperature at  $V_G = 0$  V. d) Calculated zero-bias transmission spectroscopies for all three molecular junctions, when no gate voltage is applied.

also be explained well by the theoretical transmission spectroscopies as shown in Figure 2d. Collectively, these results set the foundation for the following investigation of the dependence of the field-effect properties of molecular junctions on the molecular length and energy gap.

To explore the field-effect properties of the junctions, we placed a droplet of the ionic liquid to cover the devices (Figure 1d) and controlled the charge transport behaviors via applying different gate voltages. Specifically, we measured the current–voltage ( $I_D$ – $V_D$ ) characteristics of these three different molecular junctions at different gate voltages, changing from  $-1.5$  to  $1.5$  V with an interval of  $0.01$  V, and then compiled these gate dependent  $I_D$ – $V_D$  curves into a current ( $|I_D|$ ) mapping as a function of  $V_D$  and  $V_G$ , as shown in Figure S4 (Supporting Information). It is clear that each device exhibits obvious gate voltage-dependent current characteristics. We extracted the current values at a fixed bias voltage ( $V_D = -0.5$  V) under different gate voltages in each molecular junction and plotted the transfer curves, as shown in Figures 3a,c,e. With the change of gate voltage from  $-1.5$  to  $1.5$  V, the conductance of biphenyl molecular junctions decreases monotonically, while triphenyl and hexaphenyl molecular junctions show ambipolar conductance characteristics: first decreases and then increases with the turning point of around  $0.5$  V. To further understand such gate dependent behaviors of the junctions, two-dimensional visualizations of differential conductance ( $dI/dV$ ) plotted versus  $V_G$  and  $V_D$  for all three junctions are shown in Figures 3b,d,f,

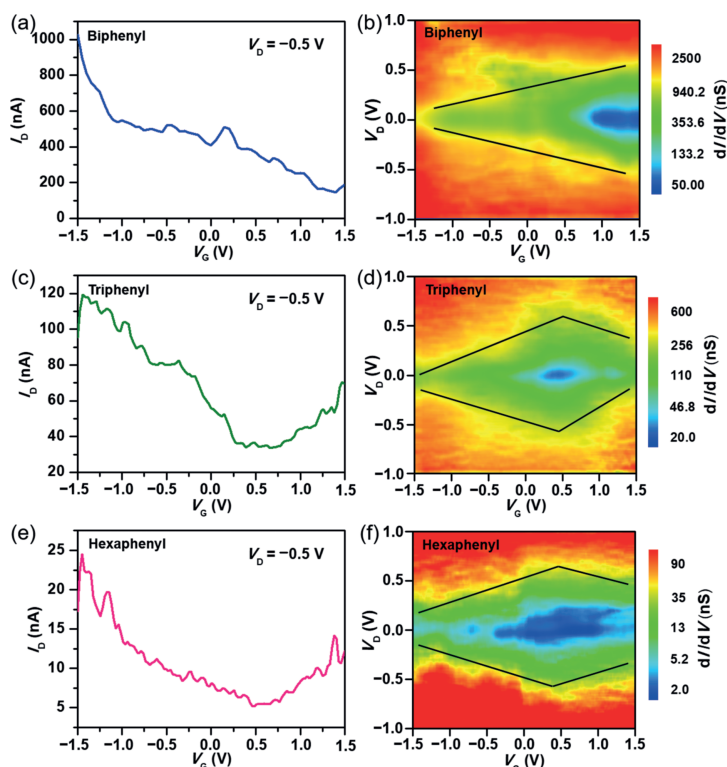


**Figure 3.** Gate-controllable charge transport in single-molecule transistors. a),c),e) Transfer characteristics for biphenyl (a), triphenyl (c), and hexaphenyl (e) molecules at  $V_D = -0.5$  V. b),d),f) Two-dimensional visualization of  $dI/dV$  versus  $V_G$  and  $V_D$  for biphenyl (b), triphenyl (d), hexaphenyl (f) molecules.

where the green-blue low conductance region is owing to off-resonant transport through the HOMO–LUMO gap and the outside red-orange high conductance region corresponds to the frontier molecular orbitals coming into the bias window. The nearly complete diamond-shaped structures can be distinguished in the conductance mapping of triphenyl and hexaphenyl molecular junctions, which demonstrate that HOMO and LUMO successively contribute to charge transport, thus leading to the ambipolar characteristics of the junctions. Figure S6 shows another set of representative data (from about 50 different functioning devices for each single-molecule junctions) showing the similar field-effect behavior, demonstrating the reproducibility and reliability.

To rule out potential artifacts, we made the similar measurements on graphene ribbons with the similar device structure, which showed totally different conductance characteristics (Figure S7) from those of molecular devices. The transfer curve in Figure S7b shows that the graphene is p-doped, resulting from the fact that the used graphene was doped during the wet transfer process.<sup>[16]</sup> In addition, as the current of graphene ribbons is much larger than that of molecular junctions, the gate response of molecular junctions should exclusively originate from the molecules.

To understand the gate-tunable conductance behaviors of molecular junctions, we consider the effect of gate potential on the alignment of the molecular frontier orbital energy levels and the Fermi level of graphene electrodes. Applying a positive potential to the gate electrode causes the aggregation of anions around the gate electrode and thus induces the build-up of corresponding cations around both the graphene electrodes and the molecular junction (Figure 1b, likewise applying negative potential to the gate electrode causes the aggregation of cations around the gate electrode and thus induces the build-up of corresponding anions around both the graphene electrodes and the molecular junction). The build-up charges around the molecule and electrodes act as a gate voltage to electrostatically shift the energy levels of molecular orbitals and Fermi level of graphene electrodes: more positive charges cause a downshift in the molecular orbitals and an increase of the graphene Fermi level; negative charges cause an upshift in the molecular orbitals and a decrease of the graphene Fermi level. As a result, this shift brings molecular LUMO closer to the graphene Fermi level and pushes molecular HOMO away from the graphene Fermi level or the HOMO closer to the graphene Fermi level and pushes molecular LUMO away from the graphene Fermi level.

To further understand the experimental observations and confirm the idea proposed above, we simulated the transport properties and their responsive behaviors to gate voltages for all three molecular junctions. The theoretical methods and device models used are detailed in the Supporting Information (Figures S8–S13). In Figures 4a,b, we give the variation of zero-bias transmission spectra under different gate voltages for triphenyl and hexaphenyl single-molecule junctions, respectively. As the gate voltage

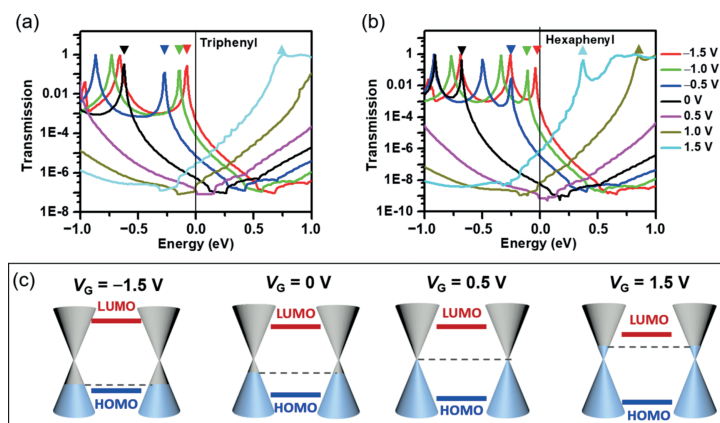


**Figure 4.** Working mechanism for graphene-molecule-graphene single-molecule transistors. a), b) Gate-dependent zero-bias transmission spectroscopies for triphenyl (a) and hexaphenyl (b) single-molecule junctions at  $-1.5 \text{ V} \leq V_G \leq 1.5 \text{ V}$  with the step of  $0.5 \text{ V}$ . The downward triangles mark p-HOMO and upward triangles mark p-LUMO. c) Energetic diagram of the alignment of molecular orbitals relative to the graphene electrode Fermi level in triphenyl and hexaphenyl single-molecule transistors under different gate voltages.

sweeps from  $-1.5$  to  $1.5 \text{ V}$ , the transmission spectra move down as a whole in energy relative to the graphene Fermi level (set to zero). In particular, when the gate voltage is smaller than  $0.5 \text{ V}$ , the transmission peak just below the graphene Fermi level, which corresponds to the perturbed HOMO (p-HOMO, marked by downward triangle in Figures 4a,b) of triphenyl/hexaphenyl molecule, resides in or near the bias window and dominates the contribution to the device conductance. With the gate voltage changing from  $-1.5$  to  $0.5 \text{ V}$ , p-HOMO gradually moves away from the graphene Fermi level, leading to the decrease of conductance. When the gate voltage further increases from  $0.5$  to  $1.5 \text{ V}$ , perturbed LUMO (p-LUMO, marked by upward triangle in Figures 4a,b) becomes closer to the graphene Fermi level and behaves as the dominant conducting molecular orbital. As p-LUMO approaches the graphene Fermi level, the conductance is gradually enhanced. Figure 4c shows a brief Scheme of energy level shift under different gate voltages, which clearly illustrates the whole picture.

For biphenyl single-molecule junctions, interfaces among biphenyl molecule, graphene electrode and ionic liquid are complex due to the small length of biphenyl molecule; and Fermi level pinning might occur as charge is transferred to biphenyl molecule (Detailed discussions are provided in the Supporting Information). Figure S15 shows the calculated zero-bias transmission spectra under different gate voltages when one hole is located at the biphenyl molecule, which correctly reproduces the experimental trend: When the gate voltage varies from  $-1.5$  to  $1.5 \text{ V}$ , p-HOMO moves away slowly from the graphene Fermi level, while p-LUMO no longer comes into the bias window, leading to the monotone decrease of conductance.

In conclusion, on the basis of the platform of GMG-SMJ, we demonstrate an efficient way to modulate both the molecular orbital energy levels and the Fermi level of graphene electrodes by using an ionic liquid as a gate dielectric, thus realizing gate-controllable charge transport.

All three electrochemically inactive aromatic chain single-molecule junctions exhibited gate-controlled conductance behavior, in which the gate efficiency was found to be largely dependent on the relationship between the molecular length and the EDL thickness. Both triphenyl and hexaphenyl molecular junctions exhibited ambipolar charge transport characteristics, resulting from the change of the dominant conducting orbital from HOMO to LUMO as the gate voltage changed from negative to positive. This is the first time of realizing ambipolar charge transport with a small gate voltage

( $|V_G| \leq 1.5 \text{ V}$ ) in electrochemically inactive molecular systems with a large energy gap ( $E_G > 3.5 \text{ eV}$ ). Therefore, this device architecture provides a reliable strategy to modulate charge transport, making an important step toward practical single-molecule transistors. As the ionic liquid can keep its EDLs unchanged below its freezing point, such single-molecule transistors can be further utilized for exploring gate-dependent quantum transport and novel physical phenomena of single molecules at cryogenic temperatures.

## Acknowledgements

We acknowledge primary financial supports from National Key R&D Program of China (2017YFA0204901 and 2016YFA0200604), the National Natural Science Foundation of China (grant 21727806 and 21688102), the Natural Science Foundation of Beijing (Z181100004418003) and the interdisciplinary medicine Seed Fund of Peking University.

## Conflict of interest

The authors declare no conflict of interest.

**Keywords:** aromatic rings · charge transport · graphene · ionic liquids · single-molecule junction

**How to cite:** *Angew. Chem. Int. Ed.* **2018**, *57*, 14222–14031  
*Angew. Chem.* **2018**, *130*, 14222–14227

- [1] A. Aviram, M. A. Ratner, *Chem. Phys. Lett.* **1974**, *29*, 277–283.
- [2] a) G. Reecht, F. Scheurer, V. Speisser, Y. J. Dappe, F. Mathevet, G. Schull, *Phys. Rev. Lett.* **2014**, *112*, 047403; b) B. Capozzi, J. L. Xia, O. Adak, E. J. Dell, Z. F. Liu, J. C. Taylor, J. B. Neaton, L. M. Campos, L. Venkataraman, *Nat. Nanotechnol.* **2015**, *10*, 522–527; c) C. Jia, A. Migliore, N. Xin, S. Huang, J. Wang, Q. Yang, S. Wang, H. Chen, D. Wang, B. Feng, Z. Liu, G. Zhang, D. Qu, H. Tian, M. A. Ratner, H. Xu, A. Nitzan, X. Guo, *Science* **2016**, *352*, 1443–1445; d) S. Thiele, F. Balestro, R. Ballou, S. Klyatskaya, M. Ruben, W. Wernsdorfer, *Science* **2014**, *344*, 1135–1138; e) F. D. Natterer, K. Yang, W. Paul, P. Willke, T. Choi, T. Greber, A. J. Heinrich, C. P. Lutz, *Nature* **2017**, *543*, 226–228; f) C. Guo, K. Wang, E. Zerah-Harush, J. Hamill, B. Wang, Y. Dubi, B. Xu, *Nat. Chem.* **2016**, *8*, 484–490; g) N. Xin, C. Jia, J. Wang, S. Wang, M. Li, Y. Gong, G. Zhang, D. Zhu, X. Guo, *J. Phys. Chem. Lett.* **2017**, *8*, 2849–2854.

- [3] a) Y. Zhang, Y. Luo, Y. Zhang, Y. J. Yu, Y. M. Kuang, L. Zhang, Q. S. Meng, Y. Luo, J. L. Yang, Z. C. Dong, J. G. Hou, *Nature* **2016**, *531*, 623–627; b) T. A. Su, H. X. Li, M. L. Steigerwald, L. Venkataraman, C. Nuckolls, *Nat. Chem.* **2015**, *7*, 215–220; c) A. C. Aragonès, N. L. Haworth, N. Darwish, S. Ciampi, N. J. Bloomfield, G. G. Wallace, I. Diez-Perez, M. L. Coote, *Nature* **2016**, *531*, 88–91; d) H. Wen, W. Li, J. Chen, G. He, L. Li, M. A. Olson, A. C. Sue, J. F. Stoddart, X. Guo, *Sci. Adv.* **2016**, *2*, e1601113; e) L. Xiang, J. L. Palma, C. Bruot, V. Mujica, M. A. Ratner, N. Tao, *Nat. Chem.* **2015**, *7*, 221–226; f) J. Park, A. N. Pasupathy, J. I. Goldsmith, C. Chang, Y. Yaish, J. R. Petta, M. Rinkoski, J. P. Sethna, H. D. Abruna, P. L. McEuen, D. C. Ralph, *Nature* **2002**, *417*, 722–725; g) M. L. Perrin, C. J. O. Verzijl, C. A. Martin, A. J. Shaikh, R. Eelkema, J. H. van Esch, J. M. van Ruitenbeek, J. M. Thijssen, H. S. J. van der Zant, D. Dulic, *Nat. Nanotechnol.* **2013**, *8*, 282–287; h) C. M. Guédon, H. Valkenier, T. Markussen, K. S. Thygesen, J. C. Hummelen, S. J. van der Molen, *Nat. Nanotechnol.* **2012**, *7*, 305–309; i) N. Xin, J. Wang, C. Jia, Z. Liu, X. Zhang, C. Yu, M. Li, S. Wang, Y. Gong, H. Sun, G. Zhang, Z. Liu, G. Zhang, J. Liao, D. Zhang, X. Guo, *Nano Lett.* **2017**, *17*, 856–861; j) J. Guan, C. Jia, Y. Li, Z. Liu, J. Wang, Z. Yang, C. Gu, D. Su, K. N. Houk, K. D. Zhang, X. Guo, *Sci. Adv.* **2018**, *4*, eaar2177; k) D. Xiang, H. Jeong, D. Kim, T. Lee, Y. Cheng, Q. Wang, D. Mayer, *Nano Lett.* **2013**, *13*, 2809–2813.
- [4] M. L. Perrin, E. Burzuri, H. S. J. van der Zant, *Chem. Soc. Rev.* **2015**, *44*, 902–919.
- [5] a) H. Song, Y. Kim, Y. H. Jang, H. Jeong, M. A. Reed, T. Lee, *Nature* **2009**, *462*, 1039–1043; b) Y. Kim, W. Jeong, K. Kim, W. Lee, P. Reddy, *Nat. Nanotechnol.* **2014**, *9*, 881–885.
- [6] a) M. L. Perrin, E. Galan, R. Eelkema, J. M. Thijssen, F. Grozema, H. S. van der Zant, *Nanoscale* **2016**, *8*, 8919–8923; b) L. Y. Hsu, N. Wu, H. Rabitz, *J. Phys. Chem. Lett.* **2014**, *5*, 1831–1836; c) X. Li, J. Hihath, F. Chen, T. Masude, L. Zang, N. Tao, *J. Am. Chem. Soc.* **2007**, *129*, 11535–11542; d) C. S. Lau, H. Sadeghi, G. Rogers, S. Sangtarash, P. Dallas, K. Porfyrakis, J. Warner, C. J. Lambert, G. A. Briggs, J. A. Mol, *Nano Lett.* **2016**, *16*, 170–176; e) L. Yuan, L. Wang, A. R. Garrigues, L. Jiang, H. V. Annadata, M. Anguera Antonana, E. Barco, C. A. Nijhuis, *Nat. Nanotechnol.* **2018**, *13*, 322–329.
- [7] D. Nesvorný, W. F. Bottke, Jr., L. Dones, H. F. Levison, *Nature* **2002**, *417*, 720–721.
- [8] E. Burzurí, Y. Yamamoto, M. Warnock, X. Zhong, K. Park, A. Cornia, H. S. J. van der Zant, *Nano Lett.* **2014**, *14*, 3191–3196.
- [9] K. Yoshida, I. Hamada, S. Sakata, A. Umeno, M. Tsukada, K. Hirakawa, *Nano Lett.* **2013**, *13*, 481–485.
- [10] a) S. Kubatkin, A. Danilov, M. Hjort, J. Cornil, J.-L. Brédas, N. Stuhr-Hansen, P. Hedegård, T. Bjørnholm, *Nature* **2003**, *425*, 698–701; b) N. J. Kay, S. J. Higgins, J. O. Jeppesen, E. Leary, J. Lycoops, J. Ulstrup, R. J. Nichols, *J. Am. Chem. Soc.* **2012**, *134*, 16817–16826; c) M. Baghernejad, X. Zhao, K. Baruel Orso, M. Fueg, P. Moreno-Garcia, A. V. Rudnev, V. Kaliginedi, S. Vesztergom, C. Huang, W. Hong, P. Broekmann, T. Wandlowski, K. S. Thygesen, M. R. Bryce, *J. Am. Chem. Soc.* **2014**, *136*, 17922–17925; d) J. A. Mol, C. S. Lau, W. J. M. Lewis, H. Sadeghi, C. Roche, A. Cnossen, J. H. Warner, C. J. Lambert, H. L. Anderson, G. A. D. Briggs, *Nanoscale* **2015**, *7*, 13181–13185.
- [11] D. Xiang, X. Wang, C. Jia, T. Lee, X. Guo, *Chem. Rev.* **2016**, *116*, 4318–4440.
- [12] K. Møth-Poulsen, T. Bjørnholm, *Nat. Nanotechnol.* **2009**, *4*, 551–556.
- [13] C. Huang, A. V. Rudnev, W. Hong, T. Wandlowski, *Chem. Soc. Rev.* **2015**, *44*, 889–901.
- [14] C. Jia, B. Ma, N. Xin, X. Guo, *Acc. Chem. Res.* **2015**, *48*, 2565–2575.
- [15] a) J. Ye, M. F. Craciun, M. Koshino, S. Russo, S. Inoue, H. Yuan, H. Shimotani, A. F. Morpurgo, Y. Iwasa, *Proc. Natl. Acad. Sci. USA* **2011**, *108*, 13002–13006; b) K. Ueno, S. Nakamura, H. Shimotani, H. T. Yuan, N. Kimura, T. Nojima, H. Aoki, Y. Iwasa, M. Kawasaki, *Nat. Nanotechnol.* **2011**, *6*, 408–412.
- [16] T. Sato, G. Masuda, K. Takagi, *Electrochim. Acta* **2004**, *49*, 3603–3611.
- [17] B. Capozzi, Q. Chen, P. Darancet, M. Kotiuga, M. Buzzeo, J. B. Neaton, C. Nuckolls, L. Venkataraman, *Nano Lett.* **2014**, *14*, 1400–1404.
- [18] Q. Xu, G. Scuri, C. Mathewson, P. Kim, C. Nuckolls, D. Bouilly, *Nano Lett.* **2017**, *17*, 5335–5341.
- [19] Y. Cao, S. Dong, S. Liu, L. He, L. Gan, X. Yu, M. L. Steigerwald, X. Wu, Z. Liu, X. Guo, *Angew. Chem. Int. Ed.* **2012**, *51*, 12228–12232; *Angew. Chem.* **2012**, *124*, 12394–12398.
- [20] E. J. Dell, B. Capozzi, J. L. Xia, L. Venkataraman, L. M. Campos, *Nat. Chem.* **2015**, *7*, 209–214.
- [21] C. Jia, X. Guo, *Chem. Soc. Rev.* **2013**, *42*, 5642–5660.

Manuscript received: June 28, 2018

Accepted manuscript online: September 14, 2018

Version of record online: October 4, 2018